

Time Frequency Analysis of EMG Signal for Gesture Recognition using Fine-grained Features

Parshuram N. Aarotale^a, Ajita Rattani^b

^aWichita State University, Dept. of Biomedical Engineering, Wichita, 67220, Kansas, USA

^bUniversity of North Texas, Dept. of Computer Science and Engineering, Denton, , Texas, USA

Abstract

Electromyography (EMG)-based hand-gesture recognition converts forearm muscle activity into control commands for prosthetics, rehabilitation, and human-computer interaction. This paper proposes a novel approach to EMG-based hand gesture recognition that uses *fine-grained* classification and presents **XMANet**, which unifies low-level local and high-level semantic cues through cross-layer mutual-attention among shallow-to-deep CNN experts. Using stacked spectrograms and scalograms derived from the Short-Time Fourier Transform (STFT) and Wavelet Transform (WT), we benchmark XMANet against ResNet50, DenseNet-121, MobileNetV3, and EfficientNetB0. Experimental results on the Grabmyo dataset indicate that, using STFT, the proposed XMANet model outperforms the baseline ResNet50, EfficientNetB0, MobileNetV3, and DenseNet121 models with improvement of approximately 1.72%, 4.38%, 5.10%, and 2.53%, respectively. When employing the WT approach, improvements of around 1.57%, 1.88%, 1.46%, and 2.05% are observed over the same baselines. Similarly, on the FORS EMG dataset, the XMANet(ResNet50) model using STFT shows an improvement of about 5.04% over the baseline ResNet50. In comparison, the XMANet(DenseNet121) and XMANet(MobileNetV3) models yield enhancements of approximately 4.11% and 2.81%, respectively. Moreover, when using WT, the proposed XMANet achieves gains of around 4.26%, 9.36%, 5.72%, and 6.09% over the baseline ResNet50, DenseNet121, MobileNetV3, and EfficientNetB0 models, respectively. These results confirm that XMANet consistently improves performance across various architectures and signal processing techniques, demonstrating the strong potential of fine-grained features for accurate and robust EMG classification.

Keywords: Electromyographic Signals, Machine Learning, Deep Learning, Fine-grained features

1. Introduction

Surface electromyogram (sEMG) signals are integral to the advancement of human-machine interface (HMI) systems. Their versatile applications span myoelectric prosthesis control [1], rehabilitative feedback systems [2], disease prediction frameworks [3], and neurorobotics [4]. In particular, sEMG-based gesture recognition has emerged as a critical component for assistive technologies in individuals with limb amputations. By enabling the precise decoding of muscle activation patterns, these systems facilitate the translation of user intent into accurate prosthetic hand

movements, thereby enhancing both the functional performance of the device and the overall user experience.

Recent advancements in hand gesture recognition have leveraged both conventional and deep learning techniques to enhance accuracy and control. Classical machine learning methods such as k-Nearest Neighbors (KNN), Linear Discriminant Analysis (LDA), and Support Vector Machines (SVM) have been effectively applied to classify hand gestures [5, 6, 7, 8, 9]. Furthermore, hybrid approaches that combine fuzzy cognitive maps (FCM) and Bayesian belief networks with extreme learning machines (ELM) have shown considerable promise in gesture classification [10]. Additionally, feature extraction strategies such as variational mode decomposition (VMD) integrated with a multiclass SVM framework and the application of fractional Fourier transform (FrFT) features with KNN have demonstrated competitive performance in discerning complex hand gestures [11, 12].

Deep learning approaches have achieved remarkable success in hand gesture recognition. Real-time systems employing deep architectures have reached accuracies of approximately 94%, often outperforming traditional models [13]. In particular, Convolutional Neural Networks (CNNs) have been extensively adopted [14, 15, 16, 17, 18], while Long Short-Term Memory (LSTM) networks have demonstrated competitive performance [19, 20, 21].

However, cross-study comparisons are often hampered by variations in experimental conditions. Differences in sensor types, sampling frequencies, and placements (e.g., elbow versus forearm) can significantly impact performance metrics, thereby limiting the generalizability of the results [9, 17, 18, 22, 23]. Hand gesture recognition using sEMG signals is inherently challenging due to high inter-class similarity and intra-class variability. Conventional CNNs, when applied to representations such as the Short-Time Fourier Transform (STFT) or wavelet transforms, may overlook subtle temporal-frequency nuances essential for fine-grained classification, as they often discard low-level details [24]. A number of studies have proposed fine-grained feature analysis for enhancing the performance of classification tasks in various domains [25, 26, 27, 28, 29]. We aim to leverage fine-grained analysis, integrating both high- and low-level features, toward accurate EMG-based hand gesture recognition, XMANet.

To address these challenges, we propose **XMANet**, a Cross-layer Mutual Attention Learning Network for fine-grained feature classification. In this framework, each convolutional layer acts as a specialized expert, autonomously identifying attention regions that emphasize discriminative features at distinct scales. These attention regions are then exchanged across layers via a mutual learning mechanism, resulting in a comprehensive feature representation that also serves as an effective form of data augmentation. This approach enhances model generalization and robustness, reducing misclassifications among similar gestures.

In summary, proposing XMANet for sEMG-based hand gesture recognition systems holds significant promise for enhancing classification accuracy and interpretability, effectively addressing key challenges in feature extraction and the inherent variability of sEMG signals. Thus, to advance the state-of-the-art in electromyography (EMG)-based gesture recognition, this paper introduces a novel framework that integrates the Fourier Transform and Time-frequency feature extraction with an innovative fine-grained version of deep learning architectures. Our approach, sEMG-XMANet, is designed to address the inherent complexities of EMG signals by leveraging advanced signal processing techniques and a multi-expert deep learning strategy. The primary **contributions** of

our work are summarized as follows:

Our Contribution:

- **Advanced Feature Extraction and Signal Representation:** Innovative techniques for processing raw EMG signals are presented. These include the segmentation and transformation of the signals into sEMG images, along with the extraction of Short-Time Fourier Transform (STFT) stacked spectrograms and time-frequency stacked scalograms, which provide enriched representations of signal dynamics.
- **Development of Novel Fine-grained Deep Learning Model (XMANet):** A deep learning model based on cross-layer mutual attention learning is developed. In this architecture, predictions are aggregated from shallow layers (capturing fine, low-level details) to deep layers (capturing high-level semantic features), with each layer treated as an independent expert to improve hand-based gesture recognition performance.
- **Experimental Validation on Latest Datasets:** Comprehensive experiments are conducted on two publicly available latest datasets, namely Grabmyo [30] and FORS-EMG [31], to validate the effectiveness of the proposed method.

This paper is organized as follows. In section 2, we discuss the related work on EMG-based gesture recognition using machine learning and deep learning models. In section 3, we discuss feature extraction techniques and In section 4 discuss proposed deep-learning architectures used in this study. In Section 5, the datasets, data pre-processing and segmentation, and evaluation metrics are discussed. The results are analyzed in section 6. Conclusions and future directions are discussed in Section 7.

2. Related Work

Recent advancements in surface electromyography (sEMG) for hand gesture recognition have seen the development of various techniques employing both traditional machine learning methods and advanced deep learning models. This section reviews the contributions of several studies in this domain.

2.1. Traditional Machine Learning Approaches

Tuncer et al. [6] applied a multilevel feature extraction approach combined with fine-tuning of k-Nearest Neighbor (kNN) and Support Vector Machine (SVM) classifiers to distinguish fifteen individual as well as combined finger movements in a publicly available dataset [7]. In a similar vein, Provakar et al. [10] introduced four hybrid models for finger movement classification. Their models included one based on graph entropy, another that utilized fuzzy cognitive maps (FCM) alongside empirical wavelet transformation (EWT), a third that merged fuzzy clustering with a least-squares support vector machine (LS-SVM) classifier, and a fourth that incorporated Bayesian belief networks (BBN) with extreme learning machines (ELM).

In another study, Essa et al. [8] evaluated five distinct sets of features using kNN, Linear Discriminant Analysis (LDA), and SVM classifiers to categorize 17 gestures, with the LDA classifier

exhibiting particularly high accuracy. Furthermore, Prabhavathy et al. [11] proposed an sEMG-based gesture classification framework that employs the Variational Mode Decomposition (VMD) technique to improve hand movement classification accuracy. Their framework used a multi-class SVM with a one-vs-one (OVO) strategy, achieving an average accuracy of 99.98%.

Similarly, Heydarzadeh et al. [32] reached an accuracy of 89% when classifying ten types of movements using an SVM classifier, with reflection coefficients serving as the feature vector. Their approach also involved estimating the Power Spectral Density (PSD) of sEMG signals from two-channel data with various window widths. Additionally, Subasi et al. [33] utilized the tunable Q-factor wavelet transform (TQWT) together with bagging and boosting ensemble classifiers to identify six different hand movements. Finally, Lee et al. [13] developed a real-time gesture recognition system for hand and finger movements based on 18 time-domain features. Their study revealed that Artificial Neural Networks (ANN) outperformed other algorithms, such as SVM, Random Forest (RF), and Logistic Regression (LR), achieving an accuracy rate of 94%.

2.2. Deep Learning Approaches

Convolutional Neural Networks (CNNs) have been extensively applied to address hand gesture recognition challenges, as demonstrated by several studies in the literature [16, 17, 18]. For example, Atzori et al. [1] employed a straightforward CNN architecture to classify nearly 50 gestures from one of the NinaPro databases, noting that the first layer’s configuration, weight initialization, data augmentation methods, and learning rate significantly affected the results. Similarly, Yang et al. [34] investigated the use of raw EMG signals as CNN input by comparing time- and frequency-domain representations on two public datasets, with especially promising outcomes on the CapgMyo-DBa dataset. Asif et al. [14] carried out a detailed analysis of the influence of various hyperparameters, such as learning rate and number of epochs, confirming that these selections are critical to convolutional neural network performance.

Chamberland et al. [22] introduced EMaGer, a scalable 64-channel HD-EMG sensor designed to accommodate different forearm sizes, and leveraged a CNN-based model for gesture classification. In addition to CNNs, LSTM networks have been used in several studies. Ghislieri et al. [23] demonstrated that LSTM networks can effectively detect muscle activity in EMG recordings without the need for background-noise computations. Moreover, Cai et al. [35] extracted both spatial and temporal features by combining CNNs with LSTM networks. Li et al. [36] proposed a CNN-LSTM architecture to classify five dynamic hand gestures across different limb positions, revealing that the model’s accuracy was affected by limb position, inter-person variability, and the choice of dynamic gestures.

Furthermore, Zhao et al. [17] incorporated fuzzy logic with LSTM networks to account for temporal correlations across EMG signal windows, successfully classifying up to four hand motions. In contrast, Antonius et al. [37] achieved promising results by merging CNNs with an LSTM-like recurrent neural network, albeit for a smaller set of basic gestures. Karman et al. [38] employed a bidirectional LSTM together with CNNs to capture both forward and backward inter-channel temporal information. Barona López et al. [39] demonstrated that a CNN-LSTM model outperforms a CNN-only approach in EMG-based hand gesture recognition, achieving a post-processed recognition accuracy of 90.55 ± 9.45 , compared to 87.26 ± 11.14 for the CNN-only model.

3. Feature Extraction Techniques: Fourier and Wavelet Transform-Based Spectrogram

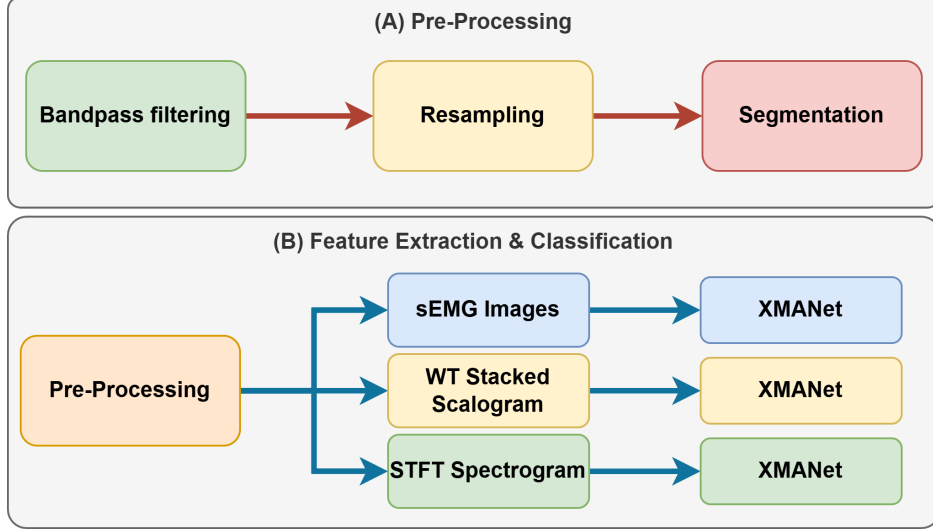


Figure 1: Figure illustrates the outline of proposed Method. A) Pre-Processing, B) Feature Extraction and Classification techniques for Gesture Recognition.

This section outlines the feature-extraction techniques employed, specifically the Short-Time Fourier Transform (STFT) and Wavelet Transform (WT), which are summarized in Fig. 1.

3.1. Short Time Fourier Transform Spectrogram

Each (sEMG) signal segment was transformed into a spectrogram using the Short-Time Fourier Transform (STFT). The Short-Time Fourier Transform (STFT) of a signal $x(t)$ is defined as:

$$\text{STFT}\{x(t)\}(m, \omega) = \int_{-\infty}^{\infty} x(t)w(t - m)e^{-j\omega t} dt \quad (1)$$

where $x(t)$ is the input signal, $w(t)$ is a window function, m is the time shift, and ω is the angular frequency [40].

The magnitude of the STFT coefficients is used to generate the spectrogram:

$$S(t, f) = |\text{STFT}\{x(t)\}(t, f)| \quad (2)$$

The logarithm of the magnitude is calculated to enhance the visibility of the signal's features:

$$\text{Log-Spectrogram}(t, f) = \log(S(t, f) + 1e - 7) \quad (3)$$

Normalization is performed to scale the log-spectrogram between 0 and 1:

$$S_{\text{norm}}(t, f) = \frac{S(t, f) - S_{\min}}{S_{\max} - S_{\min}} \quad (4)$$

where S_{\max} and S_{\min} are the maximum and minimum values of the logarithmic spectrogram, respectively [41].

This normalized log-spectrogram was converted into RGB images using a colormap and resized to 224×224 pixels to match the input size of pre-trained convolutional neural networks (CNNs). The individual channel spectrograms were stacked row-wise to form a single Spectrogram image.

3.2. Wavelet Transform based stacked scalogram

Each segmented signal was transformed into a scalogram using a continuous wavelet transform (CWT) with the Mexican hat (Mexh) wavelet.

The wavelet transform is a mathematical technique that decomposes a signal into components at various scales and positions, offering a time-frequency representation of the signal. The continuous wavelet transform (CWT) of a signal $x(t)$ is defined as

$$\text{CWT}(a, b) = \frac{1}{\sqrt{a}} \int_{-\infty}^{\infty} x(t) \psi^* \left(\frac{t-b}{a} \right) dt \quad (5)$$

where ψ is the mother wavelet, a is the scale parameter, b is the translation parameter, and ψ^* denotes the complex conjugate of ψ [42, 43]. The Mexican hat wavelet used in this study is a second derivative of the Gaussian function, providing good localization in both time and frequency domains. The scales ranged from 1 to 128 to capture the frequency components of the sEMG signals.

The power spectrum of the wavelet coefficients was calculated and normalized to enhance the signal's features. The power spectrum $P(a, b)$ is given by:

$$P(a, b) = |\text{CWT}(a, b)|^2 \quad (6)$$

Normalization was performed to scale the power spectrum between 0 and 1, which is expressed as:

$$P_{\text{norm}}(a, b) = \frac{P(a, b) - P_{\min}}{P_{\max} - P_{\min}} \quad (7)$$

where P_{\max} and P_{\min} are the maximum and minimum values of the power spectrum, respectively [44]. This normalized power spectrum was then converted into RGB images using a colormap, and resized to 224×224 pixels to match the input size of pre-trained convolutional neural networks (CNNs). The individual channel scalogram were stacked row-wise to form a single scalogram image.

4. Proposed Advanced Fine-grained Features based Methodology (XMANet)

In this section, we detail our proposed deep learning framework that exploits multi-level feature representations extracted from lower to upper layers of the CNN model. By incorporating an attention mechanism and a mutual learning strategy, our model refines feature selection and enhances learning efficacy. This approach is developed in line with the seminal contributions in fine-grained classification [45, 46, 24, 47].

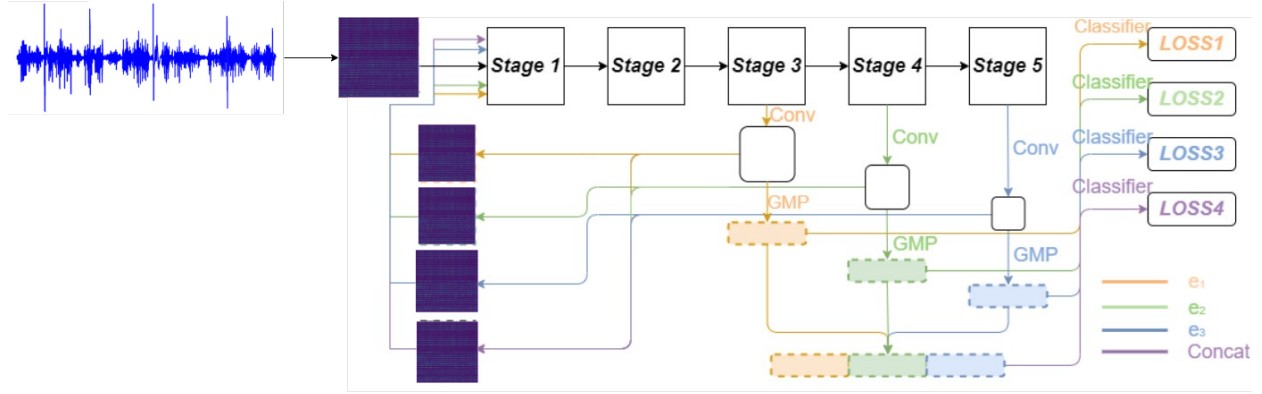


Figure 2: This figure illustrates XMANet method by introducing three experts e_1 , e_2 , e_3 , on a 5-stage backbone CNN (e.g., ResNet50). The working of each expert and the concatenation of experts are depicted in different colors. Each expert receives feature maps from a specific layer as input and generates a categorical prediction along with an attention region, which is used for data augmentation by other experts. This architecture is trained in multiple steps within each iteration. We start by training the deepest expert (e_3), followed by the shallower experts. Finally, in the last step, we train the concatenation of experts to enhance overall performance.

4.1. Expert Construction: Using Shallow to Deep Layers

In this part, we describe how a series of *experts* are derived by progressively stacking layers from a chosen backbone CNN. Any modern architecture such as ResNet50, DenseNet121, and related variants may serve as the backbone, denoted by β . Suppose β comprises M convolutional layers indexed as $\{l_1, l_2, \dots, l_m, \dots, l_M\}$, ordered from the shallowest to the deepest (fully connected layers are excluded).

We define a collection of N experts $\{e_1, e_2, \dots, e_n, \dots, e_N\}$, where each expert e_n aggregates all layers from l_1 through some l_{m_n} with $1 \leq m_n \leq M$. Consequently, the experts form a hierarchy that incrementally incorporates deeper layers, and the final expert e_N spans the complete stack l_1 to l_M .

Let the feature maps output by these experts be $\{x_1, x_2, \dots, x_n, \dots, x_N\}$, where each $x_n \in \mathbb{R}^{H_n \times W_n \times C_n}$ and H_n, W_n, C_n denote its spatial height, width, and channel count, respectively. A set of operations $\{F_1(\cdot), F_2(\cdot), \dots, F_n(\cdot), \dots, F_N(\cdot)\}$ compress these feature maps into fixed-length, one-dimensional descriptors $\{v_1, v_2, \dots, v_n, \dots, v_N\}$, where each $v_n \in \mathbb{R}^{C_v}$:

$$v_n = F_n(x_n) = f^{GMP}(x_n''), \quad (8)$$

$$x_n'' = f^{Elu}(f^{bn}(f_{3 \times 3 \times C_v/2 \times C_v}^{conv}(x_n'))), \quad (9)$$

$$x_n' = f^{Elu}(f^{bn}(f_{1 \times 1 \times C_n \times C_v/2}^{conv}(x_n))), \quad (10)$$

Here, $f^{GMP}(\cdot)$ represents global max pooling, $f^{conv}(\cdot)$ a 2-D convolution parameterized by its kernel size, $f^{bn}(\cdot)$ batch normalization, and $f^{Elu}(\cdot)$ the ELU activation. The intermediate maps x_n' and x_n'' are also utilized to derive the attention region for each expert, as detailed in Subsection 4.2.

Each expert produces a prediction score $p_n = f_n^{clf}(v_n)$ through its dedicated fully connected classifier $f_n^{clf}(\cdot)$. In addition to these individual predictions, we construct a holistic descriptor by

concatenating all expert vectors:

$$v_{oval} = f_{concat}(v_1, v_2, \dots, v_n, \dots, v_N),$$

followed by a final classifier

$$p_{oval} = f_{oval}^{clf}(v_{oval}),$$

which yields the overall prediction score for the framework.

4.2. Attention Region Prediction

Recall that x_n'' is the intermediate feature map produced by the n -th expert e_n . We consider a K -class classification task, and denote by $k_n \in \{1, 2, \dots, K\}$ the category predicted by e_n . The tensor $x_n'' \in \mathbb{R}^{H_n \times W_n \times C_n}$ serves as the basis for generating an attention region via a class-activation map (CAM) that highlights the discriminative image area for class k_n .

Class-activation map. For expert e_n , the CAM $\Omega_n \in \mathbb{R}^{H_n \times W_n}$ is computed as $\Omega_n(\alpha, \beta) = \sum_{c=1}^{C_n} p_n^c x_n''^c(\alpha, \beta)$, where (α, β) indexes spatial positions, $x_n''^c$ is the c -th channel of x_n'' , and p_n^c is the parameter of the classifier $f_n^{clf}(\cdot)$ associated with class k_n .

Upsampling and normalization. The map Ω_n is bilinearly upsampled to the input image resolution, yielding $\tilde{\Omega}_n \in \mathbb{R}^{H_{in} \times W_{in}}$ (with H_{in}, W_{in} the input height and width). We then apply min–max normalization:

$$\tilde{\Omega}_n^{norm}(\alpha, \beta) = \tilde{\Omega}_n(\alpha, \beta) - \min(\tilde{\Omega}_n) / \max(\tilde{\Omega}_n) - \min(\tilde{\Omega}_n). \quad (11)$$

Attention mask and augmentation. Pixels with positive values in the normalized map $\tilde{\Omega}_n^{norm}$ define a binary mask $\tilde{\Omega}_n^{mask}$. The corresponding region is cropped from the original image, resized back to $H_{in} \times W_{in}$, and denoted A_n . This A_n acts both as the attention region predicted by e_n and as an augmented sample for the remaining experts.

Global attention. Finally, an overall attention map A_{oval} is obtained by summing the attention information contributed by all experts, thus capturing multi-level cues across the hierarchy.

4.3. Multi-step Mutual Learning

The entire ensemble is optimized with a progressive $N+2$ -step schedule, each step minimizing the cross-entropy loss. In the first N stages the experts are updated one at a time from deepest to shallowest so that each model can refine the visual cues lying within its own receptive-field scope before being influenced by its peers. The final two stages bring the experts together: first around the shared attention regions, then around the original image.

Step 1 (deepest expert). The iteration begins by training the deepest expert e_N . Because e_N subsumes all shallower layers, this pass also yields the set of attention regions

$$\{A_1, A_2, \dots, A_n, \dots, A_N, A_{oval}\},$$

which make explicit the ‘‘specialized knowledge’’ on which each expert bases its decision.

Steps 2–N (progress toward shallow). For each subsequent expert we move upward in the hierarchy. At every step a training sample is drawn at random from a pool that contains the raw image and the attention crops proposed by *other* experts. Thus shallower experts benefit from the semantic cues revealed by deeper models, whereas deeper experts can revisit lower-level structure highlighted by their shallow counterparts.

Step N+1 (joint training on A_{oval}). All experts together with their concatenated representation are optimized in a single forward pass using the overall attention region A_{oval} . This cooperative update encourages the ensemble to integrate the diverse attention information it has accumulated and to focus on still finer-grained patterns.

Step N+2 (joint training on raw input). Finally, the concatenated descriptor is trained once more on the unaltered image so that the parameters of $f_{oval}^{clf}(\cdot)$ are well aligned with the full-resolution input, completing the mutual-learning cycle for that iteration.

Inference Phase: Figure 2 presents the prediction pipeline of the proposed model, which is equipped with $N+1$ classifiers. Given a test image, the network first outputs $N+1$ prediction scores. The image’s overall attention region is then passed through the same network, generating another $N+1$ scores. In total, $2 \times (N+1)$ scores are produced, and their arithmetic mean is taken as the final decision. This two-pass strategy improves classification accuracy by harnessing two complementary sources of evidence: (a) the ensemble of expert-specific and global predictions, and (b) features obtained from both the raw input and its corresponding attention map.

5. Experimental Validation

5.1. Datasets

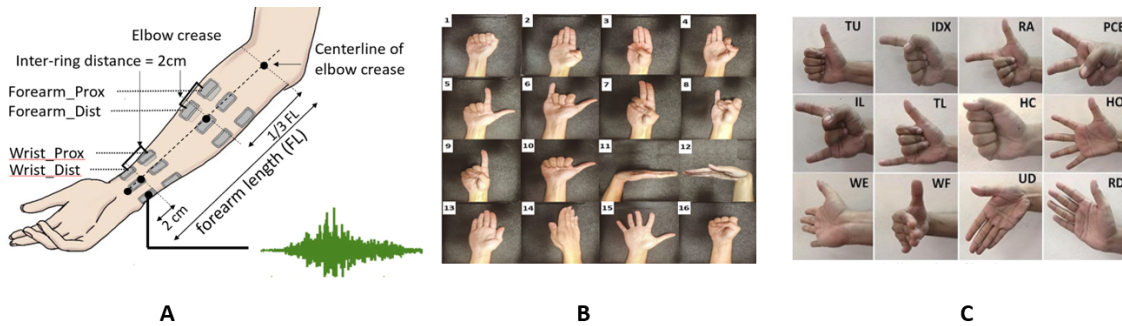


Figure 3: A) Electrode Positions [30] and B) Gesture list for Grabmyo dataset [30] and C) FORS-EMG dataset [31].

Grabmyo [30]: This dataset involves 43 healthy participants (23 males and 20 females) recruited from the University of Waterloo, with data collected on day 1, day 8, and day 29. The participants had an average age of 26.35 years (± 2.89) and an average forearm length of 25.15 cm (± 1.74 cm). Exclusion criteria included muscle pain, skin allergies, or inability to complete all sessions. The study followed ethical guidelines, with participants providing informed consent and the study being approved by the University of Waterloo’s Office of Research Ethics (31346).

The experimental setup included a PC and monitor positioned in front of a height-adjustable chair. The data was collected using an EMGUSB2+ amplifier (OT Bioelettronica, Italy) with a gain of 500 and a sampling rate of 2048 Hz, along with pre-gelled, skin-adhesive monopolar sEMG electrodes. Participants performed gestures at a normal force level, determined through trial contractions at soft, medium, and hard levels, while following visual instructions on the screen.

This dataset comprises 16 gestures, including lateral prehension, thumb adduction, various finger oppositions and extensions, wrist flexion and extension, forearm supination and pronation, hand open, and hand close. Gestures were performed in a randomized order with a ten-second rest between each. Each session included seven runs of 17 gestures (including rest), totaling 119 contractions per session. This protocol was repeated on day 8 and day 29.

FORS-EMG [31]: The FORS-EMG dataset used in this work was collected from 19 healthy individuals who performed 12 different wrist and finger motions in three different forearm orientations: pronation, neutral (rest), and supination. The participants performed five repetitions of each gesture (see Fig 3 C) while the electrodes were positioned along the mid-forearm and close to the elbow. For each gesture, eight channels (four on the forearm and four around the elbow) were used to record sEMG signals at 8 second intervals with a sampling frequency of 985 Hz. This work processes only the dataset with orientation at rest.

5.2. Preprocessing and implementation details

Surface electromyography (sEMG) signals were bandpass filtered with a frequency of 20 – 450Hz. Preprocessed signals were segmented into overlapping 0.6-second windows with a 50% overlap for feature extraction methods such as STFT Stacked Spectrogram and WT stacked Scalogram images. The data sets were divided into 70% for training and 15% each for validation and testing, and the results were reported on the test set for all experiments.

Data augmentation techniques, such as random resizing, cropping, and horizontal flipping, were applied during training to enhance the model’s robustness. Four pre-trained CNN architectures ResNet50, MobileNetV3, and DenseNet121 were fine-tuned for gesture classification by adjusting their final layers to output 17 classes for Grabmyo and 12 classes for Fors EMG dataset respectively.

Training was conducted using the Adam optimizer and cross-entropy loss function, with early stopping to prevent overfitting. The best-performing model based on validation loss was saved and evaluated on the test set, yielding accuracy metrics and detailed classification reports.

5.3. Performance Metrics

The following standard performance metrics [48] were used for the evaluation of the proposed models in this study.

$$\text{Accuracy} = \frac{T_p + T_n}{T_p + T_n + F_p + F_n} \quad (12)$$

$$\text{Precision} = \frac{T_p}{T_p + F_p} \quad (13)$$

$$\text{Recall} = \frac{T_p}{T_p + F_n} \quad (14)$$

$$F1\text{-score} = 2 \times \frac{\text{Precision} \times \text{Recall}}{\text{Precision} + \text{Recall}} \quad (15)$$

where T_p , T_n , F_p , and F_n represent true positive, true negative, false positive, and false negative recognition for the given class, respectively.

6. Results and Discussion

In this section, we discuss the results obtained by our proposed XMANet in conjunction with different backbones. For instance, XMANet (ResNet50) denotes performance of XMANet using ResNet50 backbone. The performance of XMANet is compared with existing CNN-based baselines.

6.1. Experimental Results on Grabmyo

Table 1: Gesture recognition for EMG segmented images using Deep learning CNN-based baseline and the proposed XMANet.

Models	ACC	P	R	F1
ResNet50	99.18	0.99	0.99	0.99
MobilNetV3	99.26	0.99	0.99	0.99
DenseNet121	99.44	0.99	0.99	0.99
EfficientNetB0	99.12	0.99	0.99	0.99
XMANet(ResNet50)	99.60	1.0	1.0	1.0
XMANet(DensNet121)	99.61	1.0	1.0	1.0
XMANet(MobilnetV3)	99.61	1.0	1.0	1.0
XMANet(EfficientNetB0)	99.47	0.99	0.99	0.99

The proposed XMANet leverages each pretrained CNN backbone ResNet50, DenseNet121, MobileNetV3, and EfficientNetB0 as independent specialized feature extractors. Table 1 summarizes the performance metrics for various deep learning models applied to gesture recognition

on EMG-segmented images. Notably, the DenseNet121 model achieves an accuracy of 98.44%, with precision, recall, and F1 score all at 0.99. Additionally, other pretrained models demonstrate impressive performance with accuracies of 99.18% (ResNet50), 99.26% (MobileNetV3), and 99.12% (EfficientNetB0). Furthermore, the proposed XMANet variants namely XMANet(ResNet50), XMANet(DenseNet121), XMANet(MobileNetV3), and XMANet(EfficientNetB0) deliver enhanced accuracies of 99.60%, 99.61%, 99.61%, and 99.47%, respectively, compared to their baseline counterparts.

The proposed **XMANet(ResNet50)** improved accuracy by 0.424% relative to the baseline ResNet50, by 0.342% over MobileNetV3, by 0.161% over DenseNet121, and by 0.484% over EfficientNetB0. Likewise, **XMANet(DenseNet121)** and **XMANet(MobileNetV3)** each achieved improvement of roughly 0.433%, 0.352%, 0.171%, and 0.494% compared with the respective baselines of ResNet50, MobileNetV3, DenseNet121, and EfficientNetB0.

Finally, **XMANet(EfficientNetB0)** yields improvements of 0.292%, 0.21%, 0.03%, and 0.353% over its ResNet50, MobileNetV3, DenseNet121, and EfficientNetB0 counterparts, respectively. These consistent, though marginal, improvements underscore the efficacy of the proposed modifications in refining model performance.

Table 2: Gesture recognition from STFT stacked spectrogram Images using Deep learning baselines and proposed XMANet.

Models	ACC	P	R	F1
ResNet50	91.46	0.91	0.91	0.91
MobilNetV3	85.09	0.85	0.85	0.85
DenseNet121	91.17	0.91	0.91	0.91
EfficientNetB0	88.04	0.88	0.88	0.88
XMANet(ResNet50)	93.03	0.93	0.93	0.93
XMANet(DenseNet121)	93.48	0.93	0.93	0.93
XMANet(MobilNetV3)	89.43	0.89	0.89	0.89
XMANet(EfficientNetB0)	91.89	0.92	0.92	0.92

Table 2 presents the performance metrics for various deep learning models applied to gesture recognition using STFT stacked spectrogram images. The experimental results demonstrate that the baseline models achieved accuracies of 91.46% (ResNet50), 88.04% (EfficientNetB0), 85.09% (MobileNetV3), and 91.17% (DenseNet121). With the proposed XMANet approach, these accuracies increased to 93.03% XMANet(ResNet50), 91.89% XMANet(EfficientNetB0), 89.43% XMANet(MobileNetV3), and 93.48% XMANet(DenseNet121), respectively. These enhancements underscore the efficacy of the proposed method in boosting model performance.

A detailed comparative analysis shows that the XMANet(ResNet50) model (93.03%) outper-

forms the baseline ResNet50, EfficientNetB0, MobileNetV3, and DenseNet121 models with improvements of approximately 1.72%, 5.67%, 9.33%, and 2.04%, respectively. In a similar manner, the XMANet(EfficientNetB0) model (91.89%) exhibits enhancements of 0.47% compared to the baseline ResNet50, 4.38% relative to the baseline EfficientNetB0, 7.99% over the baseline MobileNetV3, and 0.79% compared to the baseline DenseNet121. Further comparisons indicate that the XMANet(MobileNetV3) model (89.43%) achieves a 1.58% improvement relative to the baseline EfficientNetB0 and a 5.10% gain over the baseline MobileNetV3. Additionally, the XMANet(DenseNet121) model (93.48%) demonstrates gains of 2.21%, 6.18%, 9.87%, and 2.53% over the baseline ResNet50, EfficientNetB0, MobileNetV3, and DenseNet121 models, respectively. These detailed percentage improvements confirm the robustness and effectiveness of the proposed modifications across the different models.

In **summary**, XMANet model outperforms the baseline ResNet50, EfficientNetB0, MobileNetV3, and DenseNet121 models with improvements of approximately 1.72%, 4.38%, 5.10%, and 2.53%, respectively.

Table 3: Gesture recognition from Wavelet transform based stacked scalogram Images using Deep learning and proposed XMANet.

Models	ACC	P	R	F1
ResNet50	97.71	0.98	0.98	0.98
MobilNetV3	97.53	0.98	0.98	0.98
DenseNet121	97.29	0.98	0.98	0.98
EfficientNetB0	97.87	0.98	0.98	0.98
XMANet(Resnet50)	99.24	0.99	0.99	0.99
XMANet(DensNet121)	99.30	0.99	0.99	0.99
XMANet(MobilnetV3)	99.36	0.99	0.99	0.99
XMANet(EfficientNetB0)	99.28	0.99	0.99	0.99

Table 3 presents the performance metrics for various deep learning models applied to gesture recognition using wavelet transform-based stacked scalogram images. The experimental results show that the baseline models achieved accuracies of 97.71% (ResNet50), 97.87% (EfficientNetB0), 97.53% (MobileNetV3), and 97.29% (DenseNet121). The findings further demonstrate that the proposed approach significantly enhances performance over these baselines. Specifically, the proposed XMANet(ResNet50), XMANet(MobileNetV3), XMANet(DenseNet121), and XMANet(EfficientNetB0) models achieved accuracies of 99.24%, 99.36%, 99.30%, and 99.28%, respectively.

A detailed comparative analysis shows that the XMANet(ResNet50) model outperforms the baseline ResNet50, EfficientNetB0, MobileNetV3, and DenseNet121 models with improvements

of approximately 1.57%, 1.40%, 1.75%, and 2.0%, respectively.

In a similar manner, the XMANet(EfficientNetB0) model exhibits enhancements of 1.61%, 1.44%, 1.79%, and 2.05% compared to the baseline ResNet50, EfficientNetB0, MobileNetV3 and DenseNet121 respectively.

Further comparisons indicate that the XMANet(MobileNetV3) model exhibits enhancements of 1.69% compared to the baseline ResNet50, 1.52% relative to the baseline EfficientNetB0, 1.88% over the baseline MobileNetV3, and 2.13% compared to the baseline DenseNet121.

Additionally, the XMANet(DenseNet121) model demonstrates gains of 1.63%, 1.46%, 1.82%, and 2.07% over the baseline ResNet50, EfficientNetB0, MobileNetV3, and DenseNet121 models, respectively. In **summary**, the proposed models show improvements of approximately 1.57%, 1.88%, 1.46%, and 2.05% over the baseline ResNet50, MobileNetV3, DenseNet121, and EfficientNetB0 models, respectively.

The proposed XMANet enhances EMG-based gesture recognition from time-frequency (TF) images by introducing a cross-layer mutual attention mechanism. Unlike traditional CNNs that emphasize deeper semantic features, XMANet treats each CNN layer from shallow to deep as an expert capturing unique information at different abstraction levels. Shallow layers extract fine-grained frequency and temporal details, while deeper layers capture high-level semantics. Through mutual attention learning, these layers exchange attention-guided insights, enabling targeted augmentation and reducing irrelevant information. This collaboration improves feature discrimination, reduces intra-class variability and inter-class similarity, and increases robustness to real-world challenges like electrode displacement and muscle fatigue, significantly boosting recognition accuracy.

6.2. Experimental Results for FORS-EMG

Table 4: Gesture recognition for EMG-segmented Image using Deep CNN-based baseline and the proposed XMANet.

Models	ACC	P	R	F1
ResNet50	92.11	0.92	0.92	0.92
MobilNetV3	91.1	0.91	0.91	0.91
DenseNet121	94.01	0.94	0.94	0.94
EfficientNetB0	92.05	0.92	0.92	0.92
XMANet(ResNet50)	93.3	0.93	0.93	0.93
XMANet(DensNet121)	94.47	0.94	0.94	0.94
XMANet(Mobilnetv3)	93.13	0.93	0.93	0.93
XMANet(EfficientNetB0)	93.22	0.93	0.93	0.93

Table 4 presents the performance metrics for various deep learning models applied to gesture recognition for EMG segmented images tested on FORS EMG Dataset. In our experimental evaluation, the baseline models ResNet50, Mobilnetv3, Densenet121, and EfficientNetB0 achieved accuracies of 92.11%, 91.10%, 94.01%, and 92.05%, respectively. With the proposed XMANet, model ResNet50 improved to 93.30% and model DenseNet121 to 94.47%, indicating a improvement in performance for Proposed XMANet models.

A detailed comparative analysis shows that the XMANet(ResNet50) model outperforms the baseline ResNet50, EfficientNetB0, and MobileNetV3 models with improvements of approximately 1.29%, 1.36%, and 2.41%, respectively. In a similar manner, the XMANet(EfficientNetB0) model exhibits enhancements of 1.20% compared to the baseline ResNet50, 1.27% relative to the baseline EfficientNetB0, 2.33% over the baseline MobileNetV3. Further comparisons indicate that the XMANet(MobileNetV3) model exhibits enhancements of 1.11% compared to the baseline ResNet50, 1.17% relative to the baseline EfficientNetB0, 2.23% over the baseline MobileNetV3. Additionally, the XMANet(DenseNet121) model demonstrates gains of 2.56%, 2.63%, 3.70%, and 0.49% over the baseline ResNet50, EfficientNetB0, MobileNetV3, and DenseNet121 models, respectively.

In **summary**, the proposed XMANet(ResNet50) model shows improvement of approximately 1.29% over baseline ResNet50. Similarly, the proposed XMANet(DenseNet121) model exhibits an enhancement of about a 0.49% over baseline DenseNet121 . Proposed XMANET(MobileNetV3) exhibits an enhancement of about a 2.23% over baseline MobileNetV3.

The proposed XMANET(EfficientNetB0) exhibits an enhancement of about a 1.27% over baseline EfficientNetB0 .These improvements, though modest, underscore the effectiveness of the proposed XMANet in enhancing model performance.

Table 5: Gesture recognition from STFT stacked spectrogram Images using Deep learning CNN-based baseline and the proposed XMANet.

Models	ACC	P	R	F1
ResNet50	52.95	0.54	0.54	0.54
MobilNetV3	41.28	0.41	0.41	0.41
DenseNet121	54.25	0.54	0.54	0.54
EfficientNetB0	48.18	0.48	0.48	0.48
XMANet(ResNet50)	55.62	0.56	0.56	0.56
XMANet(DensNet121)	56.48	0.56	0.57	0.57
XMANet(Mobilnetv3)	42.44	0.43	0.42	0.42
XMANet(EfficientNetB0)	48.08	0.48	0.48	0.47

Table 5 presents the performance metrics for various deep learning models applied to gesture

recognition using STFT-stacked Spectrogram images tested on the FORS EMG Dataset.

In our experimental evaluation, the baseline models ResNet50, MobileNetV3, DenseNet121, and EfficientNetB0 achieved accuracies of 52.95%, 41.28%, 54.25%, and 48.18%, respectively.

The proposed XMANET achieve enhance accuracy of 55.62% ,42.44%, and 56.48% as compared to baselines ResNet50, MobileNetV3, DenseNet121 and EfficientNetB0 respectively. A detailed comparative analysis shows that the XMANet(ResNet50) model outperforms the baseline ResNet50, EfficientNetB0, MobileNetV3, and DenseNet121 models with improvements of approximately 5.04%, 15.44%, 34.73%, and 2.53%, respectively.

In a similar manner, the XMANet(EfficientNetB0) model exhibits enhancements of 0.21% relative to the baseline EfficientNetB0, 16.48% over the baseline MobileNetV3.

Further comparisons indicate that the XMANet(MobileNetV3) model exhibits enhancements of 2.81% over the baseline MobileNetV3. Additionally, the XMANet(DenseNet121) model demonstrates gains of 6.67%, 17.23%, 36.80%, and 4.11% over the baseline ResNet50, EfficientNetB0, MobileNetV3, and DenseNet121 models, respectively. **In summary**, the proposed XMANet shows an improvement of approximately 5.04% , 4.11% and 2.81% over the baseline ResNet50, DenseNet121, and MobileNetV3 models. These enhancements underscore the effectiveness of the proposed modifications in boosting model performance.

Table 6: Gesture recognition from Wavelet Transform based stacked scalogram Images using Deep learning CNN-based baseline and proposed XMANet.

Models	ACC	P	R	F1
ResNet50	54.03	0.54	0.54	0.54
MobilNetV3	47.22	0.48	0.47	0.47
DenseNet121	55.31	0.57	0.55	0.56
EfficientNetB0	49.61	0.50	0.50	0.49
XMANet(ResNet50)	56.33	0.56	0.56	0.56
XMANet(DensNet121)	60.49	0.61	0.60	0.60
XMANet(MobileNetV3)	49.92	0.50	0.50	0.50
XMANet(EfficientNetB0)	52.63	0.53	0.53	0.53

Table 6 presents the performance metrics for various deep learning models applied to gesture recognition using wavelet transform-based stacked scalogram images FORS EMG Dataset. The experimental evaluation indicates that the baseline models ResNet50, MobileNetV3, DenseNet121, and EfficientNetB0 achieved accuracies of 54.03%, 47.22%, 55.31%, and 49.61%, respectively. With the proposed XMANet, the performance improved to 56.33%, 49.92%, 60.49%, and 52.63% compared to baselines ResNet50, MobileNetV3, DenseNet121, and EfficientNetB0 respectively demonstrating a clear performance enhancement.

A detailed comparative analysis shows that **XMANet(ResNet50)** exhibits a moderate improvement over its ResNet50 baseline (a 4.26% increase) and the DenseNet121 baseline (a 1.84% increase), with a substantial gain over the MobileNetV3 baseline (a 19.29% increase) and an improvement over the EfficientNetB0 baseline (a 13.55% increase). In addition, **XMANet (DenseNet121)** delivers robust performance by achieving improvements of 11.96% over ResNet50, 28.12% over MobileNetV3, 9.36% over DenseNet121, and 21.95% over EfficientNetB0. Moreover, **XMANet (MobileNetV3)** shows a slight improvement over the MobileNetV3 baseline (a 5.72% increase) and nearly matches the EfficientNetB0 baseline (a 0.62% increase). Meanwhile, **XMANet(EfficientNetB0)** outperforms the MobileNetV3 baseline by 11.46% and records a modest gain of 6.09% over the EfficientNetB0 baseline.

In summary, the proposed XMANet exhibits an improvement of approximately 4.26%, 9.36%, 5.72% and 6.09% over the baseline ResNet50, DenseNet121, MobileNetV3 and EfficientNetB0 model. These enhancements underscore the effectiveness of the proposed modifications in boosting model performance.

7. Conclusion

This study proposed a novel pipeline for raw EMG analysis that converts signals into stacked Short-Time Fourier Transform (STFT) spectrograms and time–frequency scalograms, thereby capturing temporal dynamics with greater fidelity. Building on these enriched representations, we introduced **XMANet**, a fine-grained deep network that employs cross-layer mutual-attention learning to boost gesture-recognition accuracy.

Across the GrabMyo benchmark, XMANet consistently surpasses its baseline counterparts. With STFT, the model delivers gains of roughly 1.72%, 4.38%, 5.10%, and 2.53% over ResNet50, EfficientNetB0, MobileNetV3, and DenseNet121, respectively. On wavelet-based, it records additional improvement of about 1.57%, 1.88%, 1.46%, and 2.05% against the same baselines. For the FORS-EMG dataset, STFT experiments show XMANet(ResNet50) improved its baseline by ~5.04%, while XMANet(DenseNet121) and XMANet(MobileNetV3) improve by approximately 4.11% and 2.81%, over its baselines respectively. Using wavelet inputs, the proposed architecture secures further boosts of about 4.26%, 9.36%, 5.72%, and 6.09% over ResNet50, DenseNet121, MobileNetV3, and EfficientNetB0, respectively.

As a part of future work, a fairness-aware version of the proposed model will be implemented to evaluate and mitigate performance bias across demographic groups. Further, advanced deep learning models will be explored to capture both local and global patterns in time–frequency analysis and leveraging self-supervised learning for rich signal representations from unlabeled datasets.

References

- [1] M. Atzori, M. Cognolato, H. Müller, Deep learning with convolutional neural networks applied to electromyography data: A resource for the classification of movements for prosthetic hands, *Frontiers in neurorobotics* 10 (2016) 9.
- [2] D. K. Kumar, B. Jelfs, X. Sui, S. P. Arjunan, Prosthetic hand control: A multidisciplinary review to identify strengths, shortcomings, and the future, *Biomedical Signal Processing and Control* 53 (2019) 101588.

- [3] M. Muzammal, R. Talat, A. H. Sodhro, S. Pirbhulal, A multi-sensor data fusion enabled ensemble approach for medical data from body sensor networks, *Information Fusion* 53 (2020) 155–164.
- [4] P. Gulati, Q. Hu, S. F. Atashzar, Toward deep generalization of peripheral emg-based human-robot interfacing: A hybrid explainable solution for neurorobotic systems, *IEEE Robotics and Automation Letters* 6 (2) (2021) 2650–2657.
- [5] R. N. Khushaba, S. Kodagoda, M. Takruri, G. Dissanayake, Toward improved control of prosthetic fingers using surface electromyogram (emg) signals, *Expert Systems with Applications* 39 (12) (2012) 10731–10738.
- [6] T. Tuncer, S. Dogan, A. Subasi, Novel finger movement classification method based on multi-centered binary pattern using surface electromyogram signals, *Biomedical Signal Processing and Control* 71 (2022) 103153.
- [7] R. N. Khushaba, S. Kodagoda, Electromyogram (emg) feature reduction using mutual components analysis for multifunction prosthetic fingers control, in: 2012 12th International Conference on Control Automation Robotics & Vision (ICARCV), IEEE, 2012, pp. 1534–1539.
- [8] R. R. Essa, H. A. Jaber, A. A. Jasim, Features selection for estimating hand gestures based on electromyography signals, *Bulletin of Electrical Engineering and Informatics* 12 (4) (2023) 2087–2094.
- [9] S. Pancholi, A. M. Joshi, Portable emg data acquisition module for upper limb prosthesis application, *IEEE Sensors Journal* 18 (8) (2018) 3436–3443.
- [10] S. K. Prabhakar, D.-O. Won, Efficient strategies for finger movement classification using surface electromyogram signals, *Frontiers in Neuroscience* 17 (2023) 1168112.
- [11] T. Prabhavathy, V. K. Elumalai, E. Balaji, Hand gesture classification framework leveraging the entropy features from semg signals and vmd augmented multi-class svm, *Expert Systems with Applications* 238 (2024) 121972.
- [12] Z. Taghizadeh, S. Rashidi, A. Shalhaf, Finger movements classification based on fractional fourier transform coefficients extracted from surface emg signals, *Biomedical Signal Processing and Control* 68 (2021) 102573.
- [13] K. H. Lee, J. Y. Min, S. Byun, Electromyogram-based classification of hand and finger gestures using artificial neural networks, *Sensors* 22 (1) (2021) 225.
- [14] A. R. Asif, A. Waris, S. O. Gilani, M. Jamil, H. Ashraf, M. Shafique, I. K. Niazi, Performance evaluation of convolutional neural network for hand gesture recognition using emg, *Sensors* 20 (6) (2020) 1642.
- [15] L. Chen, J. Fu, Y. Wu, H. Li, B. Zheng, Hand gesture recognition using compact cnn via surface electromyography signals, *Sensors* 20 (3) (2020) 672.
- [16] L. Wang, J. Fu, H. Chen, B. Zheng, Hand gesture recognition using smooth wavelet packet transformation and hybrid cnn based on surface emg and accelerometer signal, *Biomedical Signal Processing and Control* 86 (2023) 105141.
- [17] W. Zhang, J. Zhang, Emg gesture recognition algorithm based on parallel multi-scale cnn, in: 2022 2nd International Conference on Frontiers of Electronics, Information and Computation Technologies (ICFEICT), IEEE, 2022, pp. 562–568.
- [18] T. Wang, W. Zhang, E. Zhou, S. Zheng, Y. Wang, G. Pang, Y. Li, An emg gesture recognition model based on batchnorm2d and incremental broad learning system, in: 2023 3rd International Conference on Frontiers of Electronics, Information and Computation Technologies (ICFEICT), IEEE, 2023, pp. 330–337.
- [19] S. E. Ovrur, X. Zhou, W. Qi, L. Zhang, Y. Hu, H. Su, G. Ferrigno, E. De Momi, A novel autonomous learning framework to enhance semg-based hand gesture recognition using depth information, *Biomedical Signal Processing and Control* 66 (2021) 102444.
- [20] O. Barron, M. Raison, G. Gaudet, S. Achiche, Recurrent neural network for electromyographic gesture recognition in transhumeral amputees, *Applied Soft Computing* 96 (2020) 106616.
- [21] I. Topalović, S. Graovac, D. B. Popović, Emg map image processing for recognition of fingers movement, *Journal of Electromyography and Kinesiology* 49 (2019) 102364.
- [22] F. Chamberland, É. Buteau, S. Tam, E. Campbell, A. Mortazavi, E. Scheme, P. Fortier, M. Boukadoum, A. Campeau-Lecours, B. Gosselin, Novel wearable hd-emg sensor with shift-robust gesture recognition using deep learning, *IEEE Transactions on Biomedical Circuits and Systems* (2023).
- [23] M. Ghislieri, G. L. Cerone, M. Knaflitz, V. Agostini, Long short-term memory (lstm) recurrent neural network for muscle activity detection, *Journal of NeuroEngineering and Rehabilitation* 18 (2021) 1–15.
- [24] D. Liu, L. Zhao, Y. Wang, J. Kato, Learn from each other to classify better: Cross-layer mutual attention learning for fine-grained visual classification, *Pattern Recognition* 140 (2023) 109550.

- [25] S. Maji, E. Rahtu, J. Kannala, M. Blaschko, A. Vedaldi, Fine-grained visual classification of aircraft, arXiv preprint arXiv:1306.5151 (2013).
- [26] G. Van Horn, P. Perona, The devil is in the tails: Fine-grained classification in the wild, arXiv preprint arXiv:1709.01450 (2017).
- [27] B. Zhao, J. Feng, X. Wu, S. Yan, A survey on deep learning-based fine-grained object classification and semantic segmentation, *International Journal of Automation and Computing* 14 (2) (2017) 119–135.
- [28] Q. Yin, W. Lu, X. Cao, X. Luo, Y. Zhou, J. Huang, Fine-grained multimodal deepfake classification via heterogeneous graphs, *International Journal of Computer Vision* 132 (11) (2024) 5255–5269.
- [29] Z. Ge, D. Mahapatra, S. Sedai, R. Garnavi, R. Chakravorty, Chest x-rays classification: A multi-label and fine-grained problem, arXiv preprint arXiv:1807.07247 (2018).
- [30] A. Pradhan, J. He, N. Jiang, Multi-day dataset of forearm and wrist electromyogram for hand gesture recognition and biometrics, *Scientific data* 9 (1) (2022) 733.
- [31] U. Rumman, A. Ferdousi, M. S. Hossain, M. J. Islam, S. Ahmad, M. B. I. Reaz, M. R. Islam, Fors-emg: A novel semg dataset for hand gesture recognition across multiple forearm orientations, arXiv preprint arXiv:2409.07484 (2024).
- [32] M. Heydarzadeh, J. Birjandtalab, M. Nourani, Emg spectral analysis for prosthetic finger control, in: 2017 European Conference on Electrical Engineering and Computer Science (EECS), IEEE, 2017, pp. 131–135.
- [33] A. Subasi, S. M. Qaisar, Surface emg signal classification using tqwt, bagging and boosting for hand movement recognition, *Journal of Ambient Intelligence and Humanized Computing* 13 (7) (2022) 3539–3554.
- [34] W. Yang, D. Yang, Y. Liu, H. Liu, Emg pattern recognition using convolutional neural network with different scale signal/spectra input, *International Journal of Humanoid Robotics* 16 (04) (2019) 1950013.
- [35] Z. Cai, Y. Zhu, A hybrid cnn-lstm network for hand gesture recognition with surface emg signals, in: Thirteenth International Conference on Digital Image Processing (ICDIP 2021), Vol. 11878, SPIE, 2021, pp. 20–28.
- [36] Q. Li, R. Langari, Emg-based hci using cnn-lstm neural network for dynamic hand gestures recognition, *IFAC-PapersOnLine* 55 (37) (2022) 426–431.
- [37] R. Antonius, H. Tjahyadi, Electromyography gesture identification using cnn-rnn neural network for controlling quadcopters, in: *Journal of Physics: Conference Series*, Vol. 1858, IOP Publishing, 2021, p. 012075.
- [38] N. K. Karnam, S. R. Dubey, A. C. Turlapaty, B. Gokaraju, Emghandnet: A hybrid cnn and bi-lstm architecture for hand activity classification using surface emg signals, *Biocybernetics and biomedical engineering* 42 (1) (2022) 325–340.
- [39] L. I. B. López, F. M. Ferri, J. Zea, Á. L. V. Caraguay, M. E. Benalcázar, Cnn-lstm and post-processing for emg-based hand gesture recognition, *Intelligent Systems with Applications* 22 (2024) 200352.
- [40] A. V. Oppenheim, R. W. Schaffer, J. R. Buck, *Discrete-Time Signal Processing*, Prentice Hall, 1999.
- [41] D. Griffin, J. Lim, Signal estimation from modified short-time fourier transform, *IEEE Transactions on Acoustics, Speech, and Signal Processing* 32 (2) (1984) 236–243.
- [42] I. Daubechies, *Ten lectures on wavelets*, SIAM, 1992.
- [43] S. Mallat, *A wavelet tour of signal processing*, Elsevier, 1999.
- [44] P. S. Addison, *The illustrated wavelet transform handbook: introductory theory and applications in science, engineering, medicine and finance*, CRC press, 2017.
- [45] M. D. Zeiler, R. Fergus, Visualizing and understanding convolutional networks, in: *Computer Vision–ECCV 2014: 13th European Conference, Zurich, Switzerland, September 6-12, 2014, Proceedings, Part I* 13, Springer, 2014, pp. 818–833.
- [46] P.-T. Jiang, C.-B. Zhang, Q. Hou, M.-M. Cheng, Y. Wei, Layercam: Exploring hierarchical class activation maps for localization, *IEEE Transactions on Image Processing* 30 (2021) 5875–5888.
- [47] A. Manzoor, A. Rattani, Fineface: Fair facial attribute classification leveraging fine-grained features, in: *International Conference on Pattern Recognition*, Springer, 2024, pp. 81–97.
- [48] T. Fawcett, An introduction to roc analysis, *Pattern recognition letters* 27 (8) (2006) 861–874.